

Supplementary Materials for

**Direct measurements of size-independent lithium diffusion and reaction times in individual polycrystalline battery particles**

Jinhong Min<sup>1</sup>, Lindsay M. Gubow<sup>1</sup>, Riley J. Hargrave<sup>2</sup>, Jason B. Siegel<sup>2</sup>, Yiyang Li<sup>1</sup>

<sup>1</sup>Materials Science and Engineering, University of Michigan, Ann Arbor, MI, USA

<sup>2</sup>Mechanical Engineering, University of Michigan, Ann Arbor, MI, USA

Corresponding author: yiyangli@umich.edu

Supplemental Tables:

Table S1. Measured capacity and electrochemical parameters for all 21 particles

Table S2. The repeatability of the electrochemical parameter quantification obtained from six consecutively conducted PITT measurements at the same voltage.

Supplemental Figures:

Fig. S1. SEM images of all 21 particles.

Fig. S2. Particle size distribution for the particles.

Fig. S3. Particle & chip assembling process.

Fig. S4. Particle volume estimation.

Fig. S5. Sensitivity analysis of the particle volume based on the particle shape assumption.

Fig. S6. Finite element analysis to estimate the electrolyte voltage drop.

Fig. S7. Propylene carbonate evaporation rate.

Fig. S8. Galvanostatic cycling of a representative particle (black) and a coin cell (red) at an approximate C-rate of C/3.

Fig. S9. Constant current and CV measurements on an empty Au working microelectrode without a particle.

Fig. S10. Multiple galvanostatic cycles of one particle on a working microelectrode.

Fig. S11. Electrochemical impedance spectroscopy (EIS) of individual particles shows negligible contact (series) resistance.

Fig. S12. A voltage and current profile of a particle over time scale during a standard experiment detailed in the Methods.

Fig. S13. Electrochemical cycling of a coin cell.

Fig. S14. To fit the PITT data, we only sample time points evenly spaced on a square root of time scale.

Fig. S15. The current traces (lighter markers) and fitting (darker lines) results for all 21 particles at all voltages.

- Fig. S16. The range of reported values and for  $j_0$  and  $D_{Li}$ .
- Fig. S17.  $D_{Li}$  and  $j_0$  plotted as a function of the experiment date.
- Fig. S18. Galvanostatic cycling of many  $\text{LiFePO}_4$  particles on a working microelectrode.
- Fig. S19. Experimental characteristic electrochemical time constants for all 21 particles at all voltages.
- Fig. S20. Cross-section SEM of pristine particles and cycled particles obtained using plasma focused ion beam (p-FIB) milling.
- Fig. S21. Computed  $D_{Li}^*$  and  $j_0^*$  estimated using different  $r_{Effective}$ .
- Fig. S22. Overpotential drop in the first cycle.
- Fig. S23. Process flow for multi-electrode array microfabrication.

Particle Number	Estimated Diameter [ $\mu\text{m}$ ]	1 <sup>st</sup> discharge Capacity [ $\mu\text{Ah}$ ]	PITT @ 4.1 V	PITT @ 4.0 V	PITT @ 3.9 V	PITT @ 3.8 V	PITT @ 3.7 V
1	5	34.6	1.34E-10	1.27E-10	5.38E-11	1.40E-10	1.53E-10
			0.039	0.032	0.030	0.041	0.031
			1.372841	1.003399	1.909268	0.594797	0.335809
2	5.5	43.5	1.85E-10	1.88E-10	1.42E-10	1.89E-10	2.31E-10
			0.023	0.022	0.023	0.034	0.034
			0.637869	0.513883	0.614877	0.39712	0.261751
3	5.9	67.5	4.57E-10	2.94E-10	2.18E-10	1.72E-10	2.07E-10
			0.097	0.077	0.065	0.068	0.046
			1.165476	1.245469	1.214266	0.943699	0.426173
4	6.8	106.2	6.95E-10	4.45E-10	3.29E-10	2.35E-10	2.66E-10
			0.143	0.114	0.096	0.093	0.056
			1.303465	1.401912	1.364592	1.099499	0.471518
5	7.4	156.8	4.35E-10	3.38E-10	2.89E-10	2.57E-10	3.19E-10
			0.100	0.087	0.079	0.091	0.059
			1.587244	1.535057	1.396902	1.065389	0.446958
6	7.4	118.1	2.30E-10	2.56E-10	2.99E-10	3.34E-10	3.62E-10
			0.044	0.034	0.031	0.045	0.046
			1.33	0.797133	0.535356	0.410643	0.310202
7	7.5	104.3	2.44E-10	2.37E-10	2.55E-10	3.16E-10	3.62E-10
			0.040	0.038	0.038	0.051	0.047
			1.137705	0.978183	0.771894	0.496615	0.321798
8	7.5	126.8	6.59E-10	4.69E-10	3.55E-10	2.47E-10	3.37E-10
			0.141	0.127	0.113	0.107	0.058
			1.48771	1.63857	1.645993	1.327207	0.420934
9	7.5	127.5	3.50E-10	3.05E-10	2.66E-10	2.92E-10	3.42E-10
			0.075	0.062	0.057	0.069	0.053
			1.499105	1.232445	1.103354	0.724674	0.381278
10	7.7	140.0	3.96E-10	3.24E-10	2.89E-10	2.78E-10	3.65E-10
			0.072	0.067	0.065	0.077	0.056
			1.307228	1.286588	1.20217	0.864667	0.386734

$D_{\text{Li}}$  [ $\text{cm}^2/\text{s}$ ] :

$j_0$  [ $\text{mA}/\text{cm}^2$ ] :

Biot Number :

Particle Number	Estimated Diameter [ $\mu\text{m}$ ]	1 <sup>st</sup> discharge Capacity [ $\mu\text{Ah}$ ]	PITT @ 4.1 V	PITT @ 4.0 V	PITT @ 3.9 V	PITT @ 3.8 V	PITT @ 3.7 V
11	8	126.1	4.18E-10	3.05E-10	2.38E-10	2.35E-10	3.73E-10
			0.115	0.099	0.084	0.092	0.064
			2.044359	2.099821	1.953374	1.273447	0.451798
12	8.4	144.4	5.73E-10	4.05E-10	3.16E-10	2.75E-10	4.11E-10
			0.135	0.118	0.099	0.102	0.066
			1.844853	1.97319	1.816965	1.267331	0.442099
13	8.5	174.4	7.14E-10	5.11E-10	3.91E-10	3.01E-10	4.32E-10
			0.158	0.139	0.118	0.115	0.065
			1.750622	1.8681	1.77291	1.320483	0.421671
14	8.7	187.5	6.05E-10	4.21E-10	3.38E-10	2.82E-10	4.46E-10
			0.127	0.113	0.103	0.109	0.067
			1.697888	1.89218	1.836514	1.368946	0.428611
15	8.8	216.5	3.90E-10	3.04E-10	2.81E-10	3.20E-10	4.67E-10
			0.097	0.083	0.075	0.090	0.066
			2.038943	1.939962	1.620937	1.006901	0.404669
16	9.5	255.79	6.30E-10	5.27E-10	4.49E-10	4.27E-10	5.73E-10
			0.105	0.097	0.087	0.092	0.065
			1.468241	1.417413	1.273688	0.834456	0.355337
17	9.9	317.5	5.20E-10	5.08E-10	4.98E-10	5.17E-10	6.19E-10
			0.057	0.056	0.061	0.085	0.069
			1.008187	0.886759	0.831872	0.661643	0.364544
18	10.1	277.8	6.43E-10	5.00E-10	4.23E-10	3.66E-10	5.66E-10
			0.164	0.144	0.131	0.148	0.087
			2.390515	2.352924	2.152045	1.658774	0.510928
19	10.7	401	1.15E-09	9.52E-10	8.03E-10	6.13E-10	6.57E-10
			0.179	0.163	0.151	0.162	0.089
			1.543315	1.478842	1.387356	1.154485	0.477487
20	11.3	468.4	9.12E-10	7.64E-10	6.85E-10	6.14E-10	7.17E-10
			0.137	0.127	0.124	0.155	0.098
			1.582658	1.518508	1.413488	1.160759	0.505174
21	12.4	607.3	1.48E-09	1.26E-09	1.08E-09	8.20E-10	8.85E-10
			0.203	0.192	0.183	0.197	0.104
			1.578105	1.525255	1.445607	1.214495	0.477753

$D_{\text{Li}}$  [ $\text{cm}^2/\text{s}$ ] :

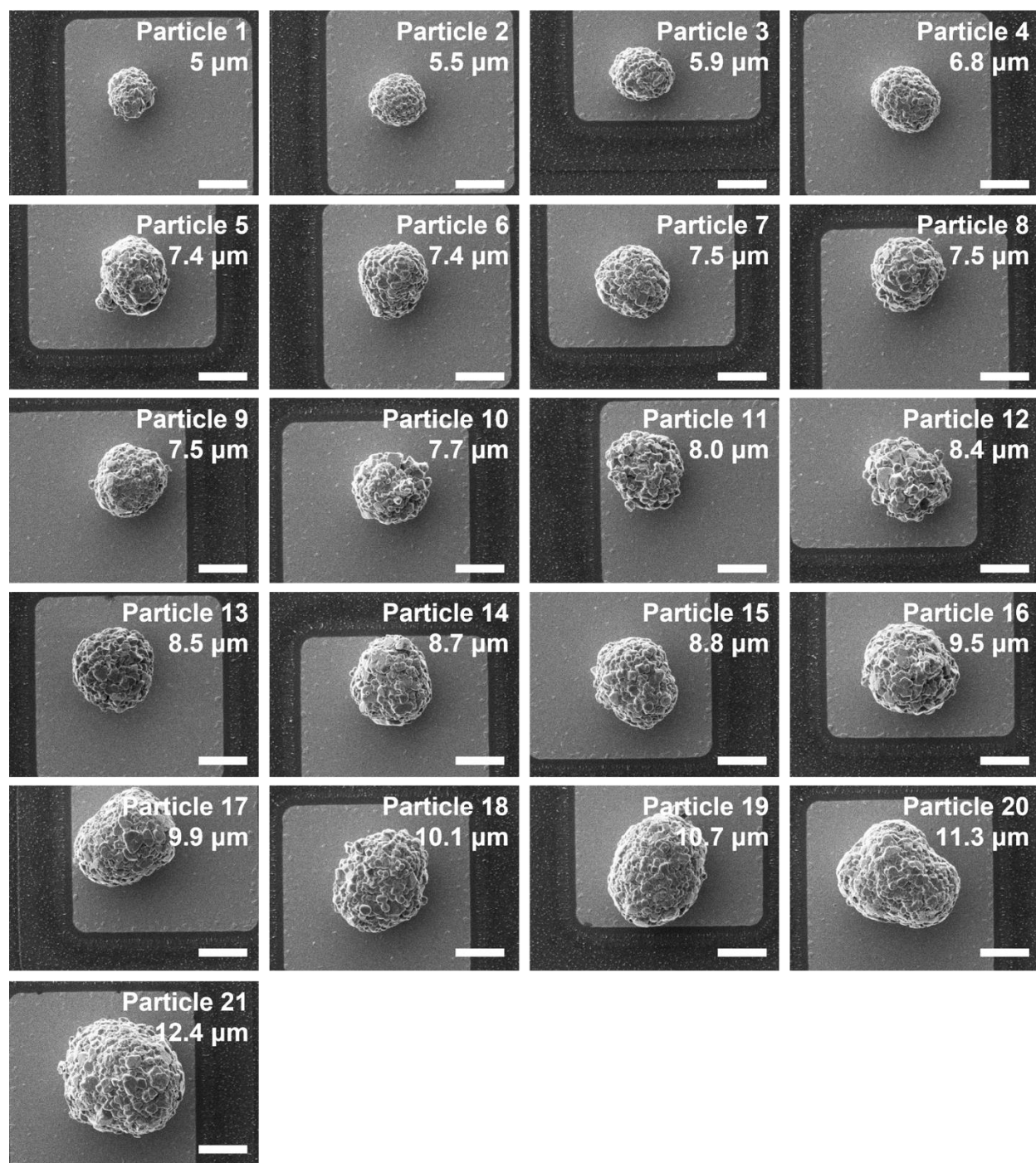
$j_0$  [ $\text{mA}/\text{cm}^2$ ] :

Biot Number :

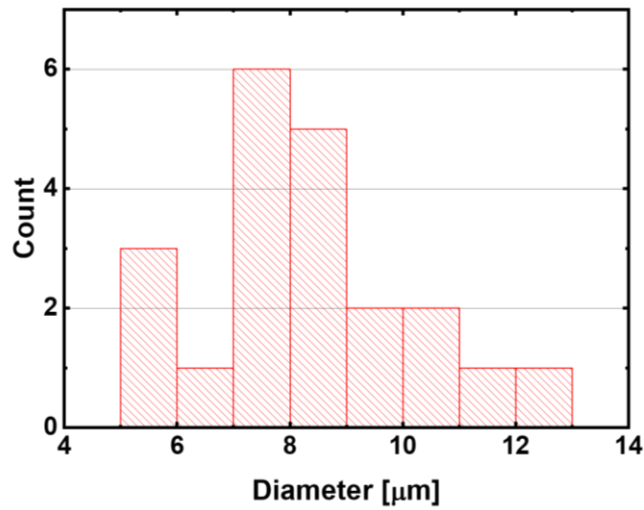
**Table S1.** Measured capacity and electrochemical parameters for all 21 particles

	$D_{Li}$ @ 4.1 V [cm <sup>2</sup> /s]	$j_0$ @ 4.1 V [mA/cm <sup>2</sup> ]	$D_{Li}$ @ 4.0 V [cm <sup>2</sup> /s]	$j_0$ @ 4.0 V [mA/cm <sup>2</sup> ]	$D_{Li}$ @ 3.9 V [cm <sup>2</sup> /s]	$j_0$ @ 3.9 V [mA/cm <sup>2</sup> ]	$D_{Li}$ @ 3.8 V [cm <sup>2</sup> /s]	$j_0$ @ 3.8 V [mA/cm <sup>2</sup> ]	$D_{Li}$ @ 3.7 V [cm <sup>2</sup> /s]	$j_0$ @ 3.7 V [mA/cm <sup>2</sup> ]
<b>Trial 1</b>	6.24E-10	0.046	6.52E-10	0.043	6.70E-10	0.045	7.37E-10	0.062	8.48E-10	0.061
<b>Trial 2</b>	6.19E-10	0.041	6.63E-10	0.041	6.71E-10	0.044	7.42E-10	0.061	8.32E-10	0.060
<b>Trial 3</b>	6.08E-10	0.042	6.84E-10	0.040	6.90E-10	0.043	7.43E-10	0.061	8.38E-10	0.060
<b>Trial 4</b>	6.16E-10	0.041	6.86E-10	0.039	6.98E-10	0.042	7.49E-10	0.060	8.38E-10	0.059
<b>Trial 5</b>	6.36E-10	0.040	6.70E-10	0.039	6.86E-10	0.042	7.61E-10	0.059	8.38E-10	0.059
<b>Trial 6</b>	6.37E-10	0.039	6.92E-10	0.038	6.95E-10	0.041	7.55E-10	0.058	8.37E-10	0.059
<b>Mean</b>	6.23E-10	0.042	6.75E-10	0.040	6.85E-10	0.043	7.48E-10	0.060	8.38E-10	0.060
<b>Standard deviation (Std)</b>	1.2E-11	0.0026	1.5E-11	0.0018	1.2E-11	0.0015	9E-12	0.0013	5E-12	0.0006
<b>Std / Mean [%]</b>	1.9 %	6.2 %	2.3 %	4.7 %	1.8 %	3.5 %	1.2 %	2.1 %	0.6 %	1.0 %

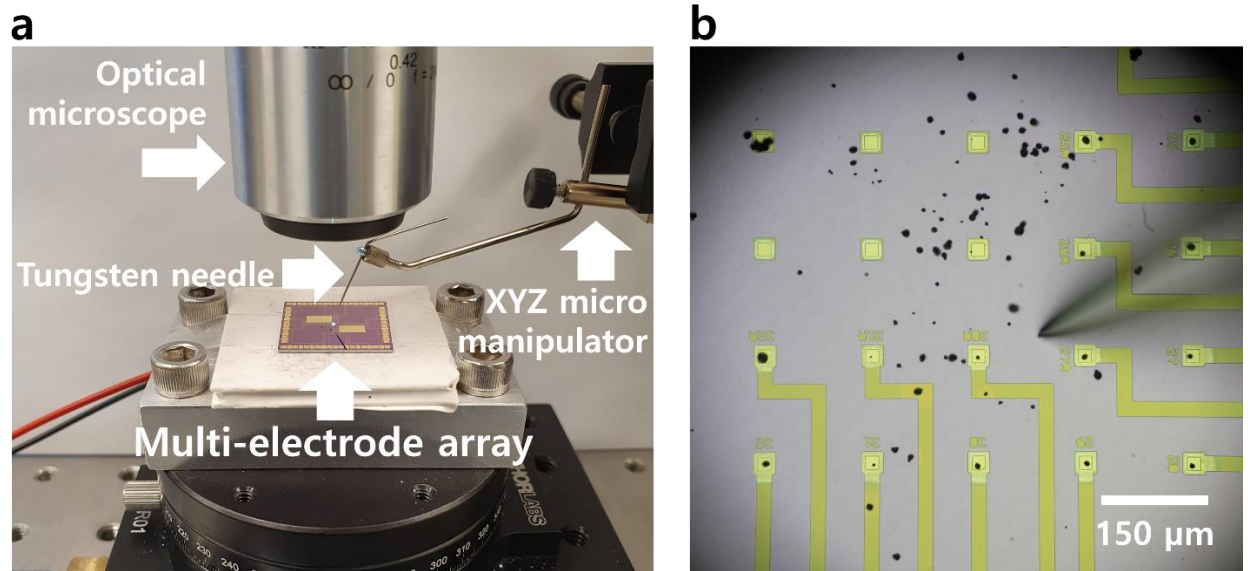
**Table S2. The repeatability of the electrochemical parameter quantification obtained from six consecutively conducted PITT measurements at the same voltage.** Our results show a standard deviation 0.5-2% for  $D_{Li}$  and from 1-6% for  $j_0$ .



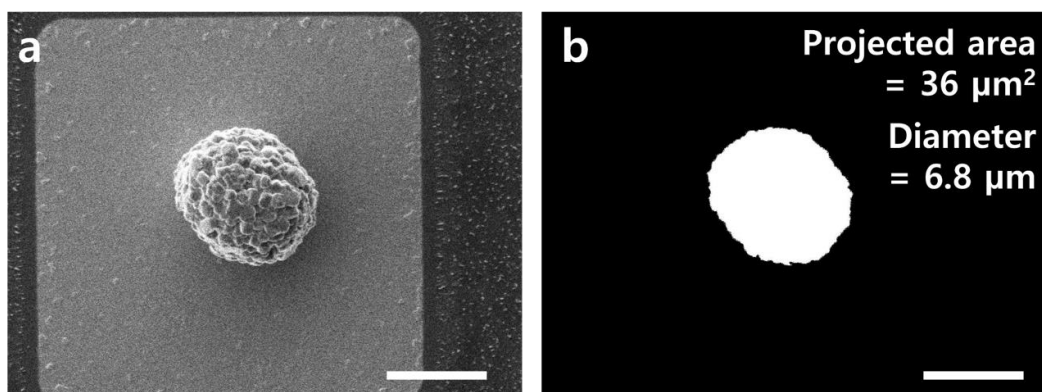
**Fig. S1. SEM images of all 21 particles.** The scale bars in each image equal 5  $\mu\text{m}$



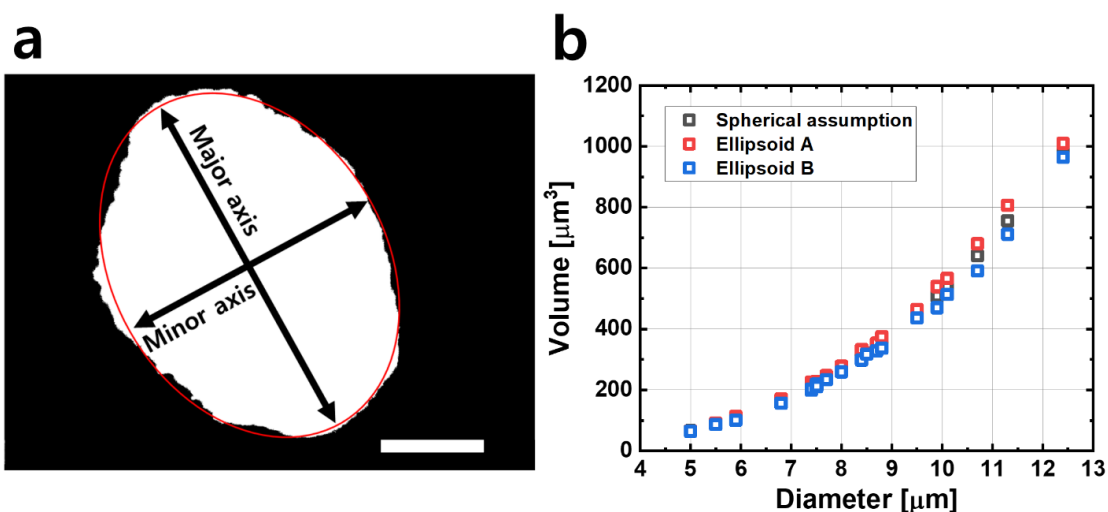
**Fig. S2. Particle size distribution for the particles.** This chart shows the diameter distribution for the 21 particles measured in this work.



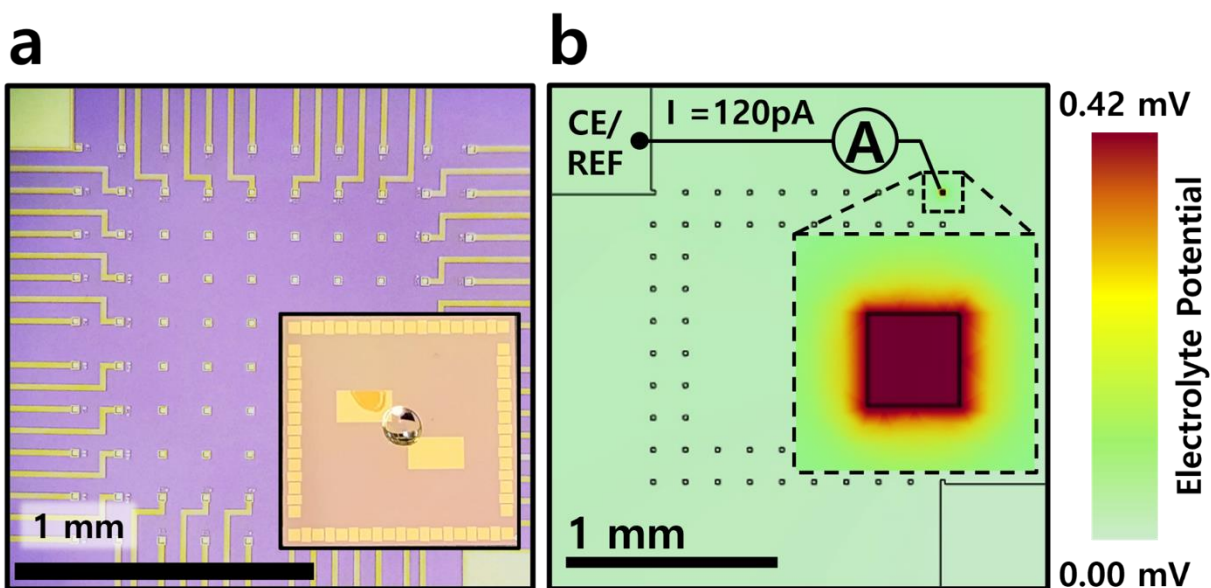
**Fig. S3. Particle & chip assembling process** a) Experimental setup for particle positioning on a multi-electrode array using an xyz micro-manipulator and optical microscope. b) Optical micrograph of the tungsten needle and randomly scattered particles during the particle positioning process.



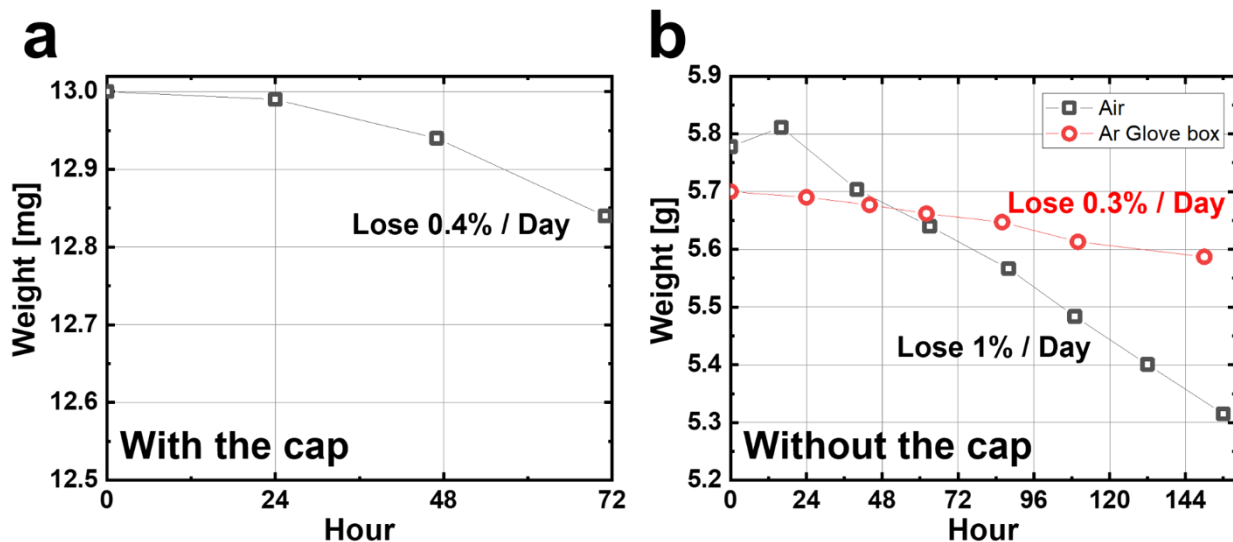
**Fig. S4. Particle volume estimation** a) SEM image of a NMC532 particle on a working microelectrode. b) Processed SEM image thresholded using Adobe Photoshop. The particle region is colored white and the other regions are colored black. The number of white pixels is counted using Matlab and translated into projected area and diameter. The scale bars in each image equal 5  $\mu\text{m}$ . The diameter of the particle is calculated based on the assumption that  $Area = \pi r^2$ , where the radius  $r$  is half the diameter.



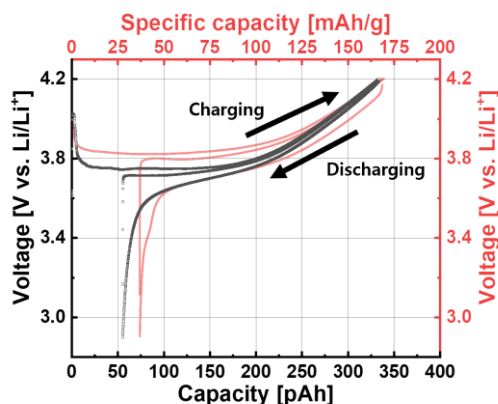
**Fig. S5. Sensitivity analysis of the particle volume based on the particle shape assumption** a) Thresholded SEM image to estimate the projected area of a secondary particle. The red line indicates an ellipsoid fitting of the particle. The fitting gives the length of the major axis and minor axis of the ellipsoid. The scale bar in the image equals 5  $\mu\text{m}$  b) The volume of particles calculated using ellipsoid and spherical assumption. Under the spherical assumption used in the main text, we assume that the volume is given by  $Volume = \frac{4}{3}\pi r^3$ , where the radius  $r$  is calculated from the 2D projected area using  $Area = \pi r^2$ . Under ellipsoid assumption, we use the equation  $Volume = \frac{4}{3}\pi abc$ , where  $a$  is half the major axis diameter, and  $b$  is half the minor axis diameter, and  $c$ , which cannot be viewed from the projections, either equals  $a$  (red) or  $b$  (blue). Regardless of the assumption, there is little difference in the estimated volume.



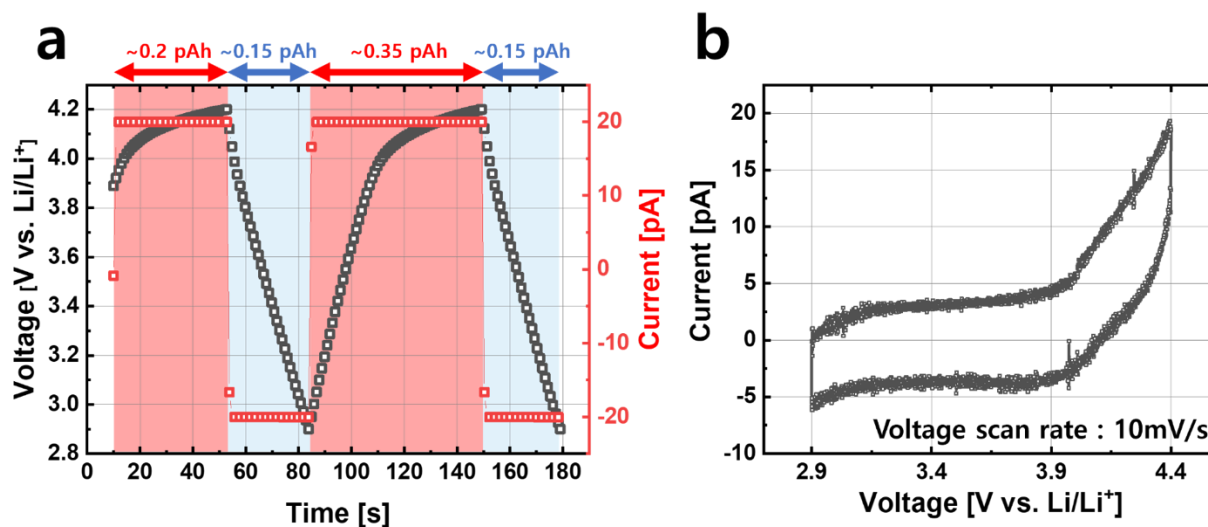
**Fig. S6. Finite element analysis to estimate the electrolyte voltage drop** a) Optical microscopic image of working microelectrodes and counter/reference electrodes in the region of interest for the finite element analysis. The inset shows  $3\mu\text{l}$  electrolyte dropped on the multi-electrode array taken with a digital camera. b) Results of 3D finite element modeling of the liquid electrolyte based on an electrical current resistance model. The model assumes that the conductivity and thickness of the electrolyte are  $6\text{ mS cm}^{-1}$  and  $0.1\text{ mm}$ , respectively. To compute the highest voltage drop, we compute the voltage drop between a CE/REF and the working microelectrodes furthest away from the CE/REF. Because the largest current used in this experiment is  $200\text{ pA}$ , the electrolyte potential drop cannot be larger than  $1\text{ mV}$ . The finite element model based on COMSOL is included in the Data Archive. The electrolyte conductivity for  $1\text{M LiPF}_6$  in PC ( $6\text{ mS cm}^{-1}$ ) was taken from M. Ding & T. R. Jow. "Conductivity and Viscosity of PC-DEC and PC-EC Solutions of  $\text{LiPF}_6$ . *J. Electrochem Soc.*, 150, A620 (2003)



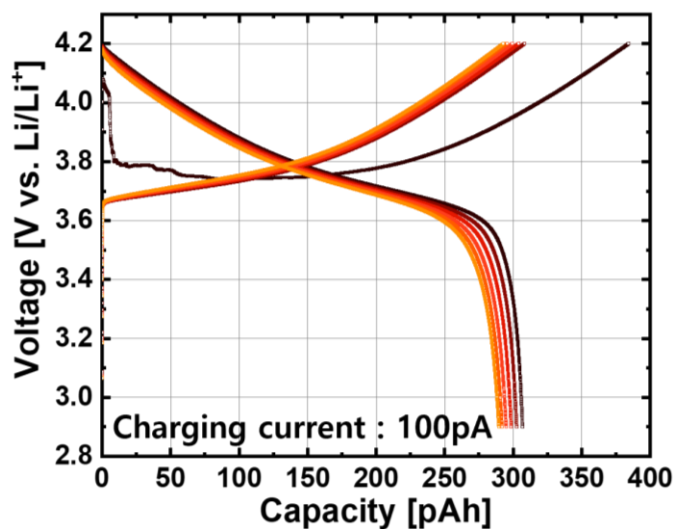
**Fig. S7. Propylene carbonate evaporation rate** **a)** The liquid propylene carbonate with a stainless steel cap evaporates  $\sim 0.4\%$ /day in the ambient atmosphere. The  $\sim 12$  mg electrolyte in this experiment is comparable to the  $\sim 4$  mg of electrolyte in single-particle electrochemical experiments. **b)** The non-negligible amounts of propylene carbonate vapor in the glovebox substantially reduce the propylene carbonate evaporation rate in the glovebox; however, it is difficult to precisely measure milligrams of electrolyte in a glovebox. Combined, we estimate that no more than  $0.5\%$  of the electrolyte evaporates every day in the glovebox. Over an eight-day experiment, we anticipate no more than  $5\%$  of the electrolyte will have evaporated.



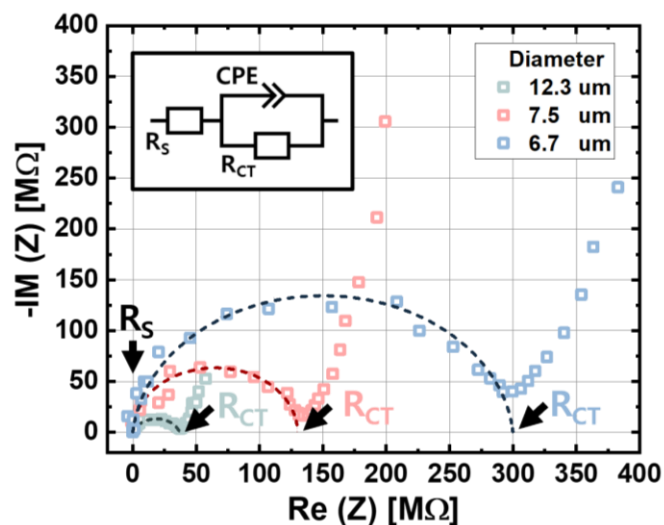
**Fig. S8. Galvanostatic cycling of a representative particle (black) and a coin cell (red) at an approximate C-rate of C/3.** The first charge, second discharge, and second charge curves of the representative NMC particle and coin cell are superimposed on each other. The particle was (dis)charged between 2.9 and 4.2 V at a constant 120 pA. The coin cell with an active NMC mass of 25.5 mg was (dis)charged between 2.9 and 4.2 V at a constant  $47.1 \text{ mA}_{\text{NMC}}^{-1}$ .



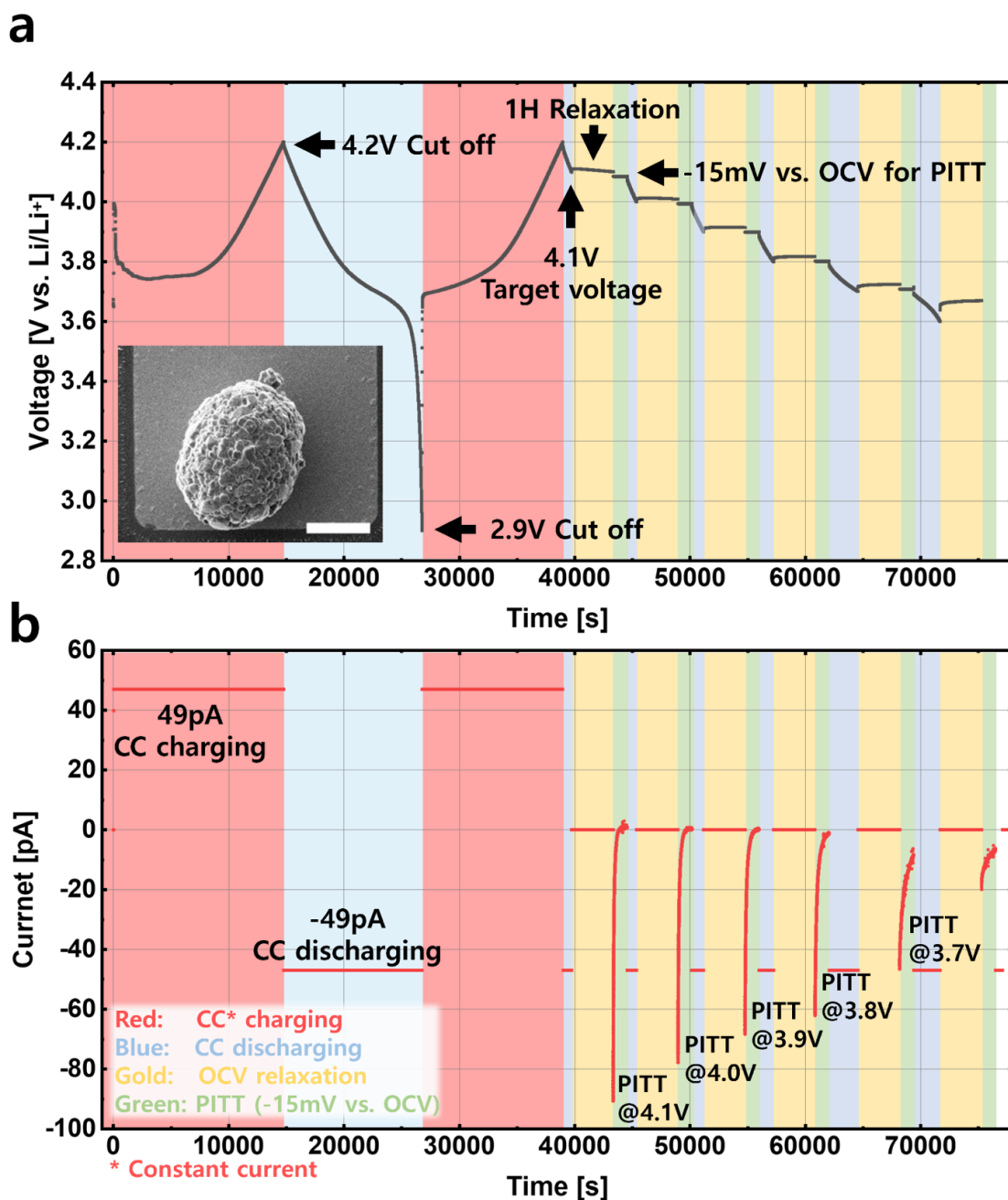
**Fig. S9. Constant current and CV measurements on an empty Au working microelectrode without a particle** a) 20 pA of constant current charge and discharge cycle was repeated on a blank working microelectrode twice. The negligible amount of discharge capacity,  $\sim 0.15$  pAh, compared to the discharge capacity of NMC532 particles was measured. b) Result of cyclic voltammetry measurement an empty Au working microelectrode. The parasitic current is  $\sim 5$  pA at 4.2V, which is the highest voltage used for this experiment.



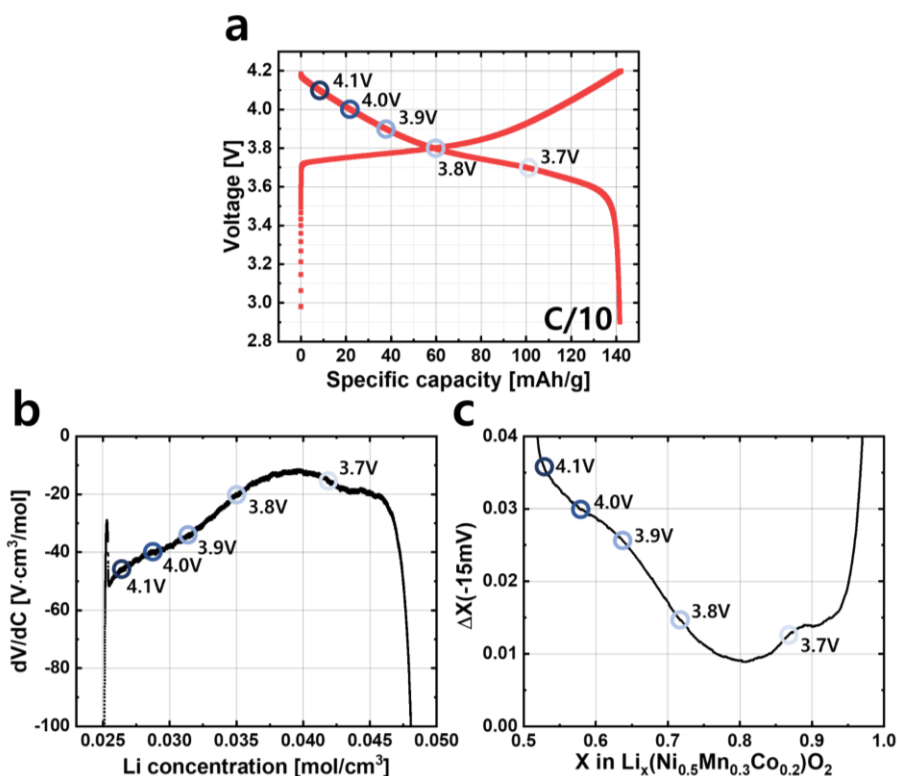
**Fig. S10. Multiple galvanostatic cycles of one particle on a working microelectrode.** This particle was cycled between 4.2 V and 2.9 V under a charging current of 100 pA for six times. After the first charging cycle, subsequent charging and discharging voltage profiles are stable.



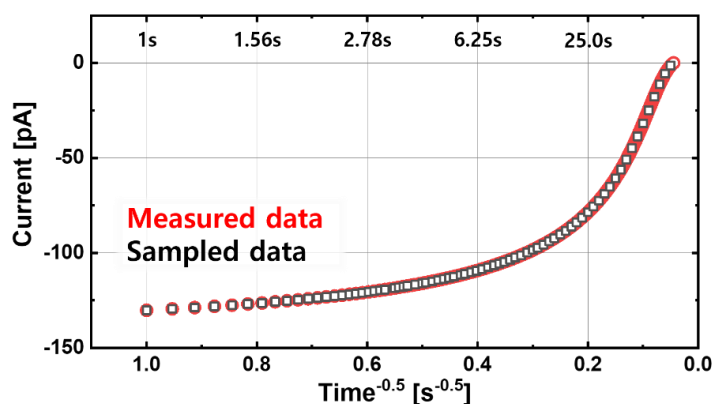
**Fig. S11. Electrochemical impedance spectroscopy (EIS) of individual particles shows negligible contact (series) resistance.** Electrochemical impedance spectroscopy (EIS) of different particles (squared points) and their fittings (dashed lines). The EIS frequency ranged from 1 kHz to 1 mHz; the amplitude was 25 mV conducted at 3.9 V. The inset equivalent circuit was used for the fitting. The series resistance,  $R_s$  is negligible compared to charge transfer resistance,  $R_{CT}$ , confirming negligible contact resistance between the particle and the Au microelectrode. Due to non-negligible parasitic capacitance from the wires, it is difficult to fit the Warburg diffusion element, which is why we primarily used PITT to obtain electrochemical parameters.



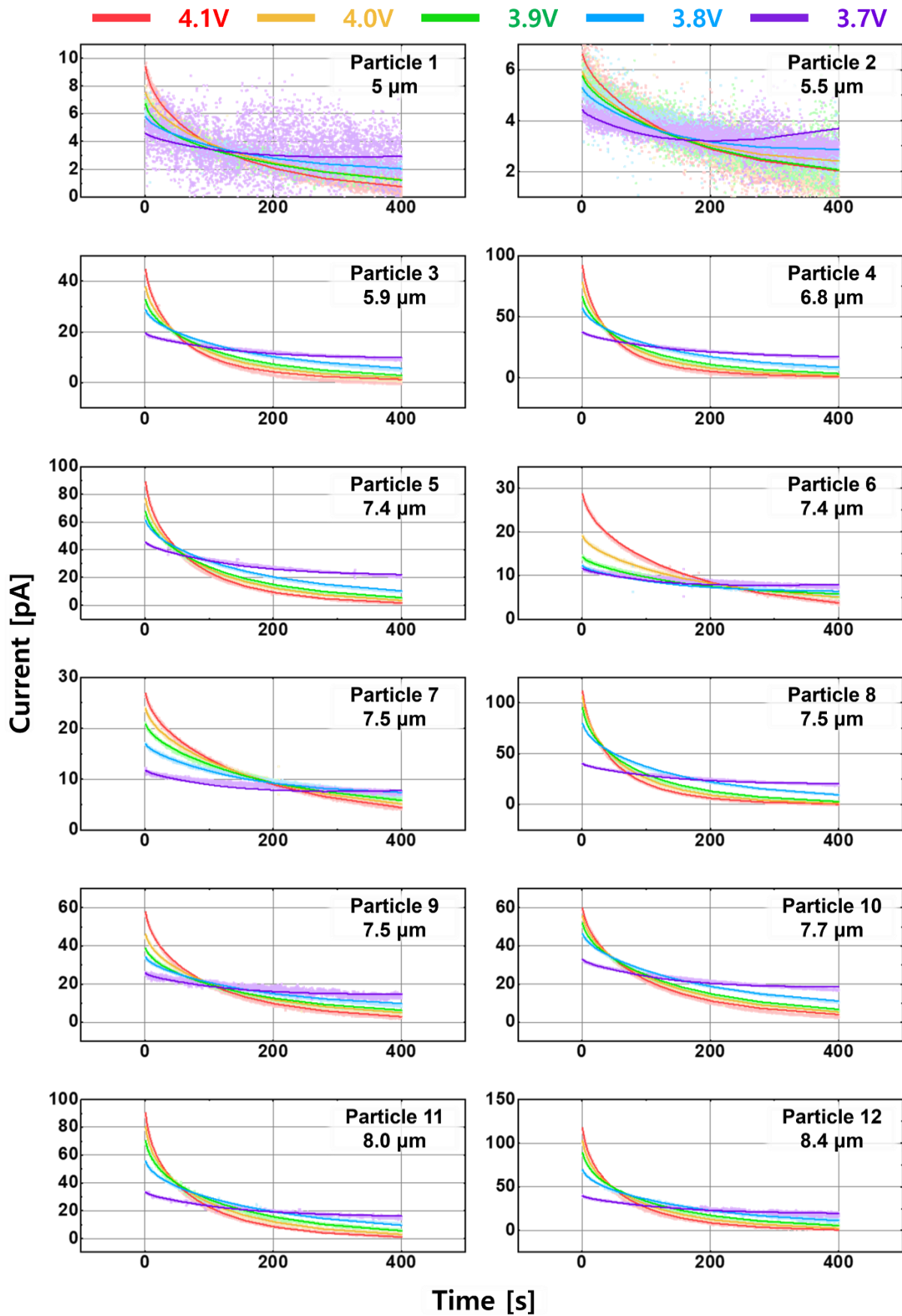
**Fig. S12.** A voltage and current profile of a particle during a standard experiment detailed in the **Methods**. The first ~39,000 s consist of the first charge, first discharge, and second charge used to estimate capacity (Fig. 2). The next 38,000 s contain the PITT measurements used to calculate  $j_0$  and  $D_{Li}$ . **a)** The voltage profile of the particle. The inset image is an SEM image of the particle used in this measurement. The scale bar in the image equals 5  $\mu\text{m}$  **b)** A current profile of a particle during electrochemistry. Along with the particle discharging, the absolute initial PITT current decreases, and the time for the current decay increases.



**Fig. S13. Electrochemical cycling of a coin cell** **a)** The charging/discharging of NMC532/Li coin cell cycling curves. The coin cell was charged to 4.2 V and discharged to 2.9 V under C-rate of C/10. **b)** Derivative of voltage during the discharge of the coin cell as a function of Li concentration. The  $dV/dC$  value for every 100 mV step from 4.1 V to 3.7 V was used to estimate  $j_0$ .  $C$  here represents the molar lithium concentration of lithium in the solid. **c)** The change in the lithium fraction  $X$  that is associated with a 15mV change in the electrochemical potential.



**Fig. S14.** To fit the PITT data, we only sample time points evenly spaced on a square root of time scale. This sampling strategy minimizes the bias of data at longer time intervals and yielded better fits to eq (1,2).



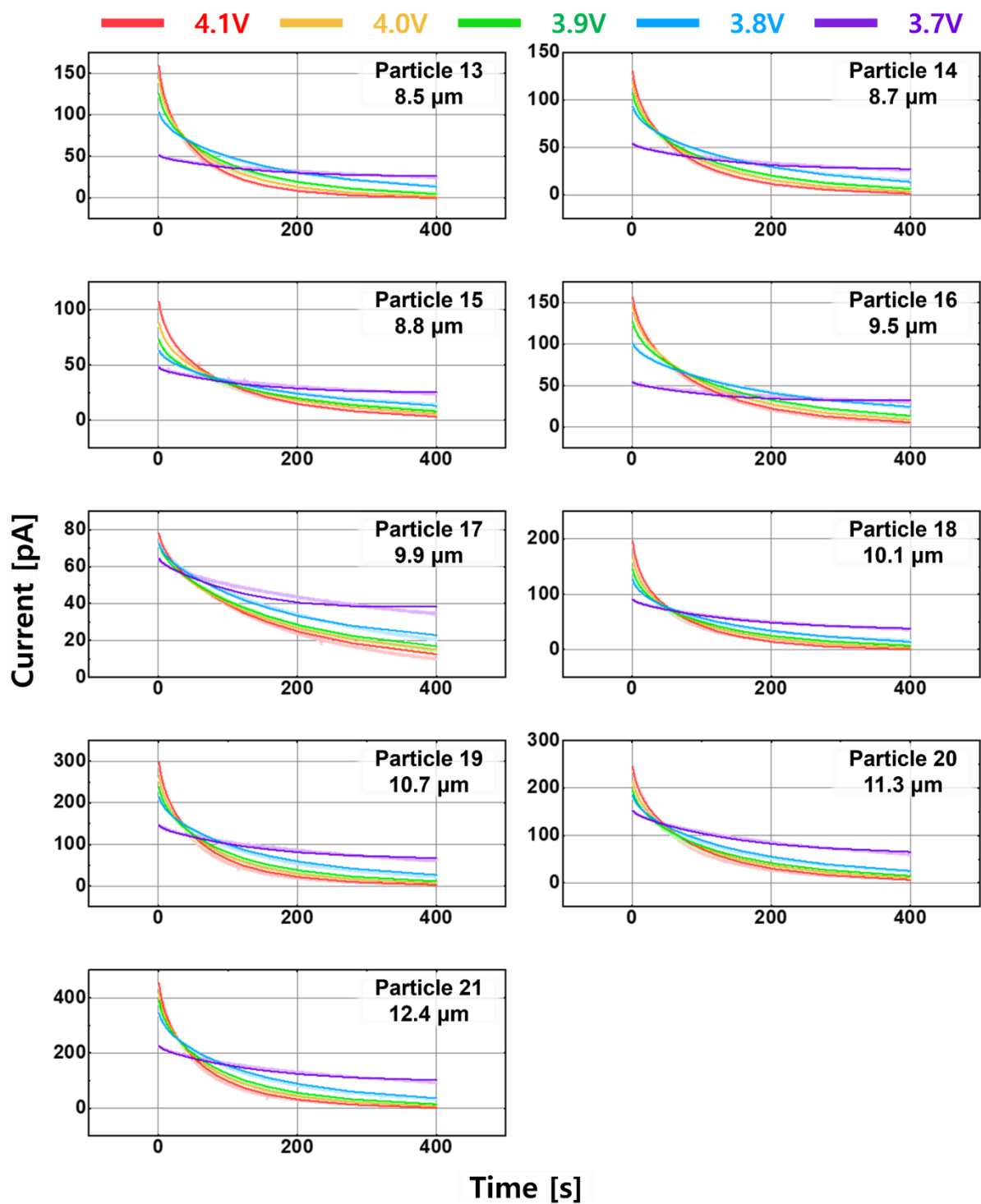
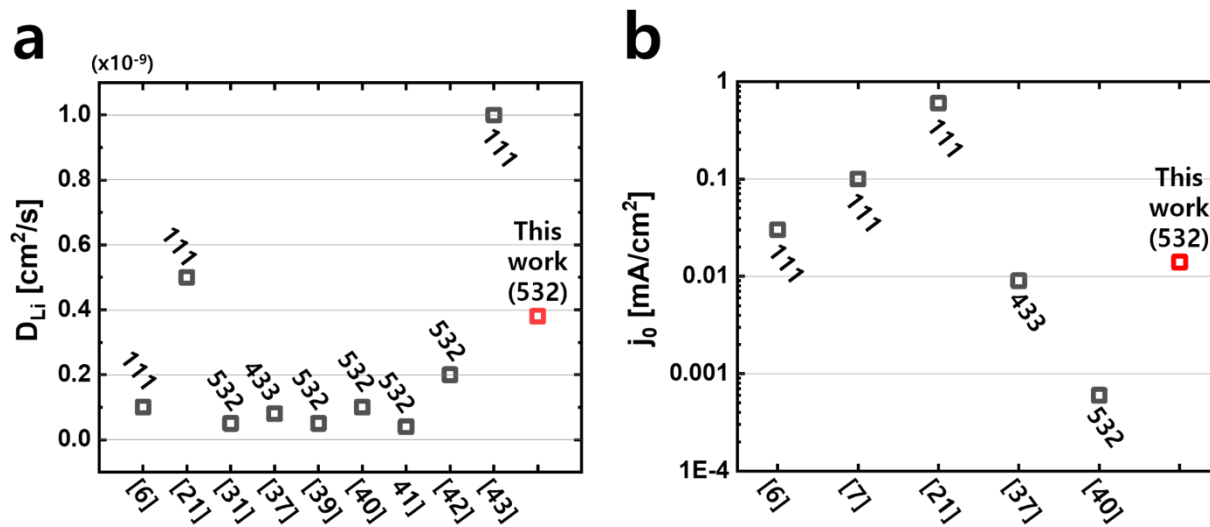
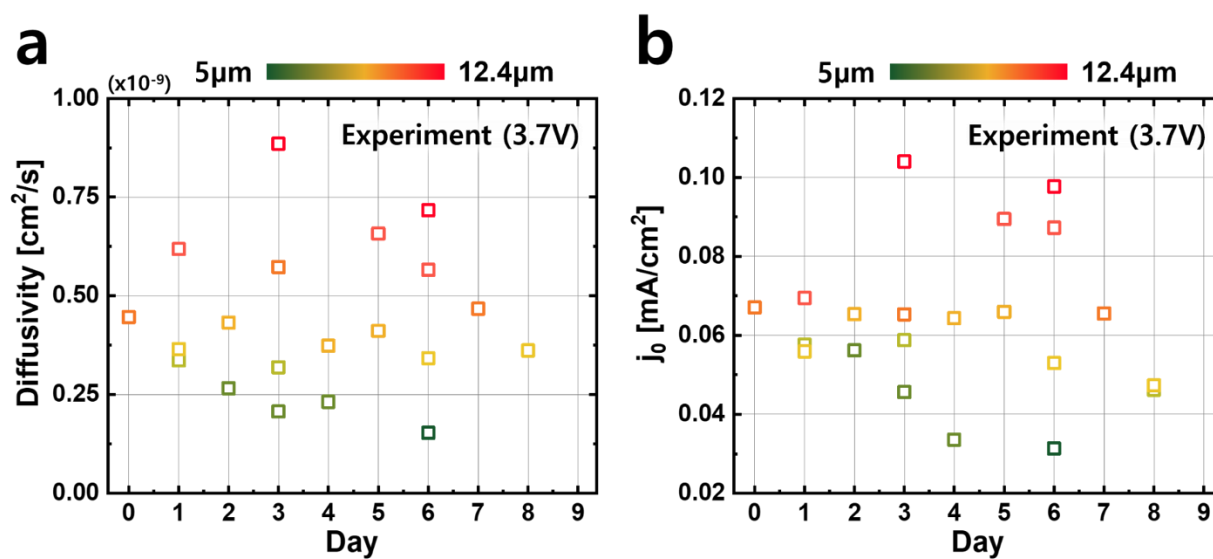


Fig. S15. The current traces (lighter markers) and fitting (darker lines) results for all 21 particles at all voltages.



**Fig. S16. The range of reported values and for  $j_0$  and  $D_{Li}$**  a,b)  $j_0$  and  $D_{Li}$  were extracted at SOC of  $\sim 50\%$ , or  $\text{Li}_{0.5}(\text{Ni}_x\text{Mn}_y\text{Co}_z)\text{O}_2$ . Our average extracted values plotted here are broadly consistent with reported  $j_0$  and  $D_{Li}$ . The three numbers next to the markers indicate the [xyz] ratio of the transition metals. The x-axis label indicates the reference number from the main text. The values plotted here assume the conventional model whereby lithium enters the secondary particle surface and diffuses into the bulk (Fig. 6a).



**Fig. S17.  $D_{Li}$  and  $j_0$  plotted as a function of the experiment date** a, b) The  $D_{Li}$  and  $j_0$  is extracted at 3.7V and plotted with time. The color of symbols indicates the diameter of particles. Up to 4 particles were successfully tested and cycled on each day.

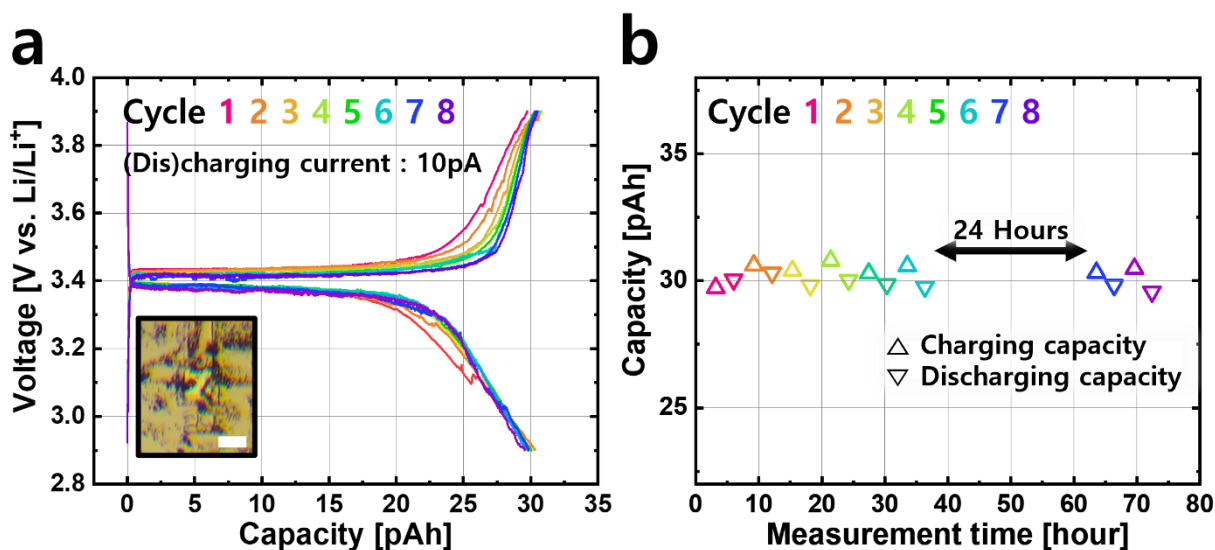


**Fig. S18. Galvanostatic cycling of many LiFePO<sub>4</sub> particles on a working microelectrode.** a) To conduct electrochemistry on LiFePO<sub>4</sub>, we placed many LiFePO<sub>4</sub> particles (~200 nm each) on a working microelectrode. These particles were (dis)charged between 2.9 and 3.9 V at a constant 10 pA. After six cycles of charge and discharge, the particles were left at open circuit for 24 hours, followed by an additional two cycles of charge and discharge. The inset shows an optical image of many LiFePO<sub>4</sub> particles being cycled; the scale bar is 20 μm. b) (Dis)charging capacity of many LiFePO<sub>4</sub> particles on a working microelectrode along with time. No significant degradation was observed between these two sets of cycles.

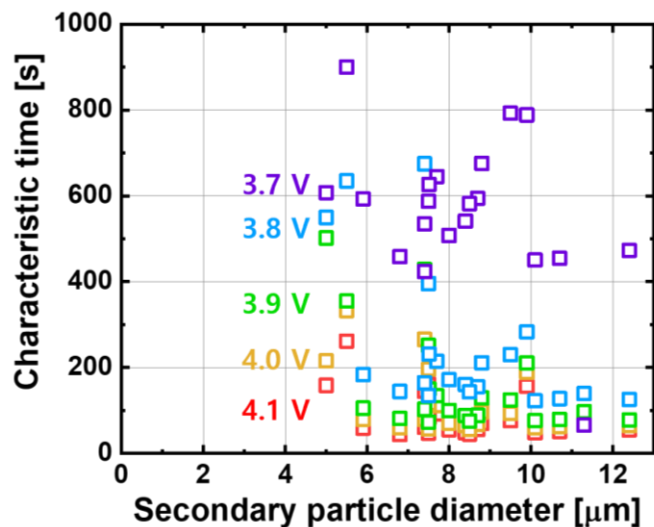


**Fig. S19. Experimental characteristic electrochemical time constants for all 21 particles at all voltages.** The characteristic time represents the amount of time it takes for the PITT current to decay to  $\exp(-1)$  of the initial current value. Although the characteristic time depends on voltage, we did not observe any correlation with particle size at all measurement voltages.

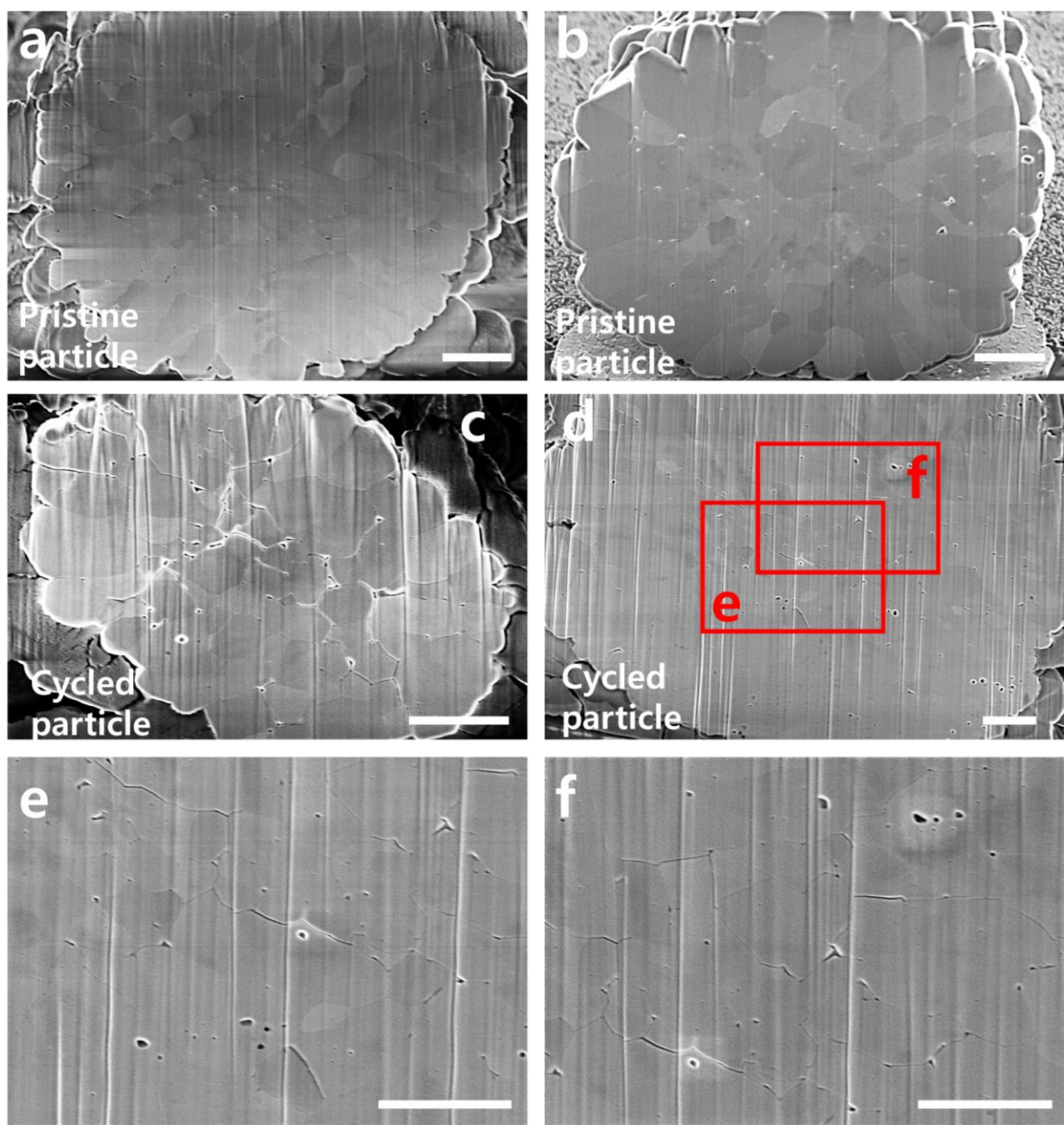


**Fig. S20. Cross-section SEM of a, b) pristine particles and c, d) cycled particles obtained using plasma focused ion beam (p-FIB) milling (see Methods for details). e, f) Higher-resolution SEM images highlights cracks in a cycled particle. The scale bars in all images equal 1  $\mu\text{m}$ . The vertical streaks are curtaining artifacts from the pFIB cross-section.**

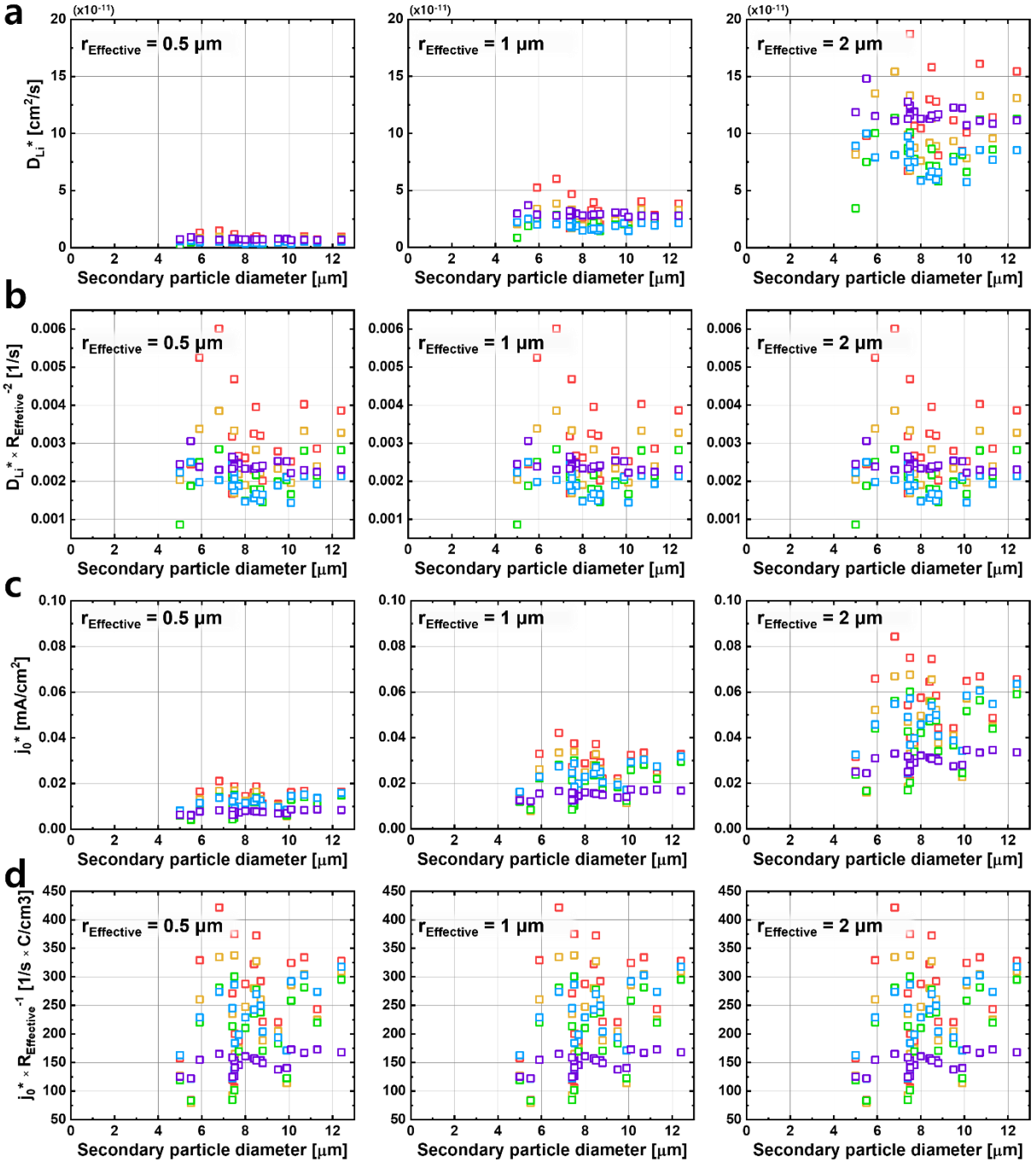


**Fig. S21. Computed  $D_{Li}^*$  and  $j_0^*$  estimated using different  $r_{Effective}$ .** **a, c)**  $D_{Li}^*$  and  $j_0^*$  estimates under the condition that  $r_{Effective}$  equals 0.5  $\mu\text{m}$ , 1  $\mu\text{m}$ , and 2  $\mu\text{m}$ . Note that larger  $r_{Effective}$  increases  $D_{Li}^*$  quadratically and increases and  $j_0^*$  linearly. **b, d)** We find that  $D_{Li}^* r_{Effective}^{-2}$  and  $j_0^* r_{Effective}^{-1}$  are constant values regardless of the  $r_{Effective}$  chosen.  $D_{Li}^* r_{Effective}^{-2}$  has units of  $[\text{s}^{-1}]$ , while  $j_0^* r_{Effective}^{-1}$  has units of  $[\text{A cm}^{-3}]$ , which equals  $[\text{s}^{-1} \text{C cm}^{-3}]$ . Because the charge of a battery particle scales with the volume,  $j_0^* r_{Effective}^{-1}$  also effectively has units of  $[\text{s}^{-1}]$ . These time units reflect the fact that PITT data only captures representative reaction and diffusion timescales, and that the electrochemical parameters can only be obtained if we know the effective radius a priori.

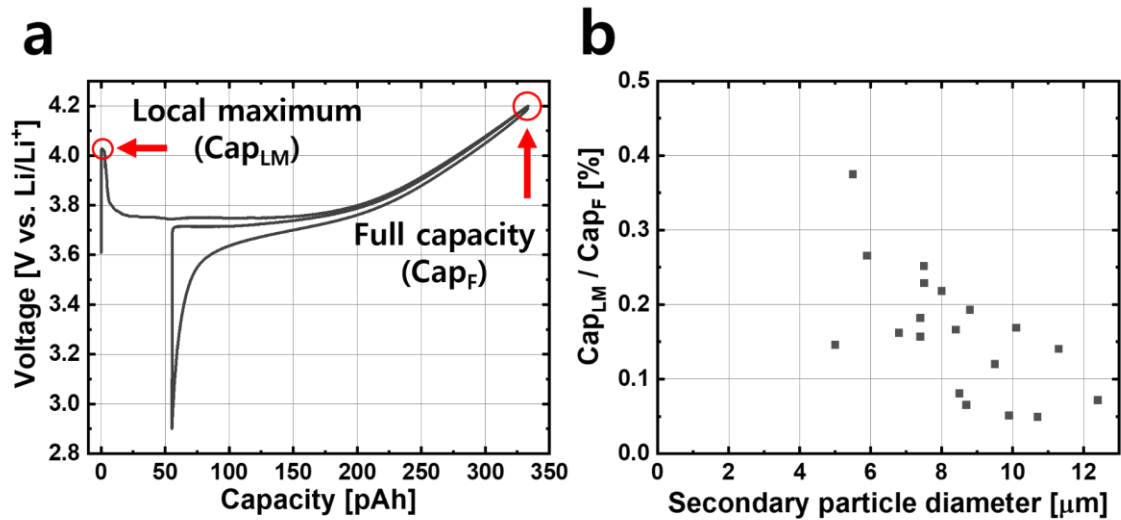


**Fig. S22: Overpotential drop in the first cycle.** a) Galvanostatic cycling shows a clear drop in the overpotential at the very beginning, with a defined local minimum. We hypothesize that this overpotential drop is a result of the particle cracking and the increase in the electrochemically-active surface area. b) This voltage drop occurs at less than 1% of the state of charge.

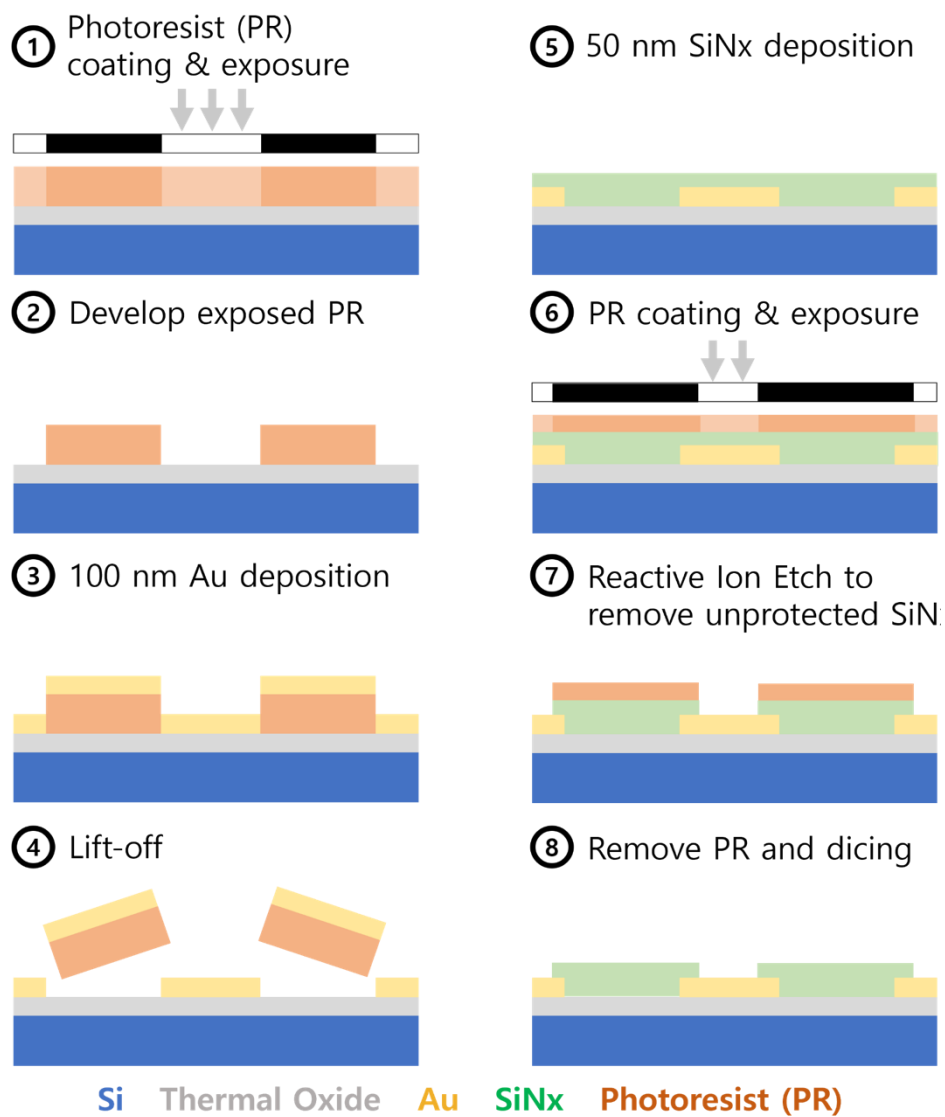


**Fig. S23. Process flow for multi-electrode array microfabrication.** The fabrication was conducted in the Lurie Nanofabrication Facility at the University of Michigan.